International Journal for Modern Trends in Science and Technology
Volume 12, Issue 05, pages 421-433
ISSN: 2455-3778 online
Available online at: http://www.ijmtst.com/vol12issue05.html
DOI: https://doi.org/10.5281/zenodo20567898

Enhanced Smart Mobile Power Bank with Wind–PV–HESS Integration and Adaptive ANN Control for Mobile Microgrids

Dr. J. Srinu Naick | D. Nandavardhan Reddy | K. Suresh | T. Sangeetha | B. Sai Prasuna

Department of Electrical and Electronics Engineering, Chadalawada Ramanamma Engineering College, Tirupati, Andhra Pradesh, India.

To Cite this Article
Dr. J. Srinu Naick, D. Nandavardhan Reddy, K. Suresh, T. Sangeetha & B. Sai Prasuna (2026). Enhanced Smart Mobile Power Bank with Wind–PV–HESS Integration and Adaptive ANN Control for Mobile Microgrids, International Journal for Modern Trends in Science and Technology, 12(05), 421-433. https://doi.org/10.5281/zenodo20567898

Article Info
Received: 07 May 2026; Revised: 26 May 2026; Accepted: 30 May 2026.

KEYWORDS

Smart Mobile Power Bank (SMPB),
Wind–PV Hybrid System,
Hybrid Energy Storage System (HESS),
Adaptive Neural Network (ANN) Control,
DC Microgrid,
Alternative Fuel Vehicles (AFVs),
Mobile Charging Station (MCS)

ABSTRACT

This paper presents an improved Smart Mobile Power Bank (SMPB) architecture that integrates wind power generation with conventional photovoltaic (PV) systems and hybrid energy storage systems (HESS) to enhance operational stability and reduce grid dependency in mobile dc microgrids under high penetration of alternative fuel vehicles (AFVs). Conventional SMPB systems relying solely on PV, HESS, and virtual inertia control (VIC) exhibit limitations during low solar availability and rapidly varying vehicle charging demands. To overcome these challenges, a compact wind energy conversion system (WECS) is incorporated, forming a hybrid wind–PV–HESS structure capable of providing a more reliable and flexible renewable energy supply. An adaptive artificial neural network (ANN)–based controller is employed to improve dc-bus voltage regulation, enhance dynamic response, and mitigates transient disturbances arising from sudden AFV charging or discharging events. The ANN controller learns system behavior online and adaptively coordinates power flow among the WECS, PV array, HESS, and grid interface converters, demonstrating superior stabilization performance compared to conventional VIC-based control. The proposed SMPB functions both as a mobile charging station (MCS) and a grid-supportive dc machine, offering improved voltage smoothing, inertia response, and ancillary support to weak or heavily loaded grids. Simulation results indicate that the wind-assisted SMPB with adaptive ANN control enhances system stability, reduces transient oscillations, improves renewable energy utilization, and minimizes reliance on the utility grid. This study provides a simulation-based validation of a resilient and efficient solution for future power systems with high AFV integration.

1. Introduction

The rapid growth of alternative fuel vehicles (AFVs), electric vehicles (EVs), and renewable energy technologies has significantly transformed modern power systems. Increasing environmental concerns, depletion of fossil fuel resources, and stringent carbon-emission regulations have accelerated the adoption of sustainable transportation and clean energy infrastructures [1], [2]. Consequently, the demand for reliable, efficient, and flexible charging solutions has become a major research focus in smart grid and microgrid applications. Mobile charging infrastructures capable of supporting AFVs while reducing dependence on conventional utility grids are emerging as promising solutions for future energy systems [3]. Among various approaches, the Smart Mobile Power Bank (SMPB) has gained considerable attention as a portable energy platform that can function both as a mobile charging station (MCS) and as an auxiliary power support unit for distribution networks [4]. SMPBs are generally composed of renewable energy sources, energy storage systems, and power electronic converters integrated within a mobile framework. Their ability to deliver charging services in remote locations, emergency situations, and areas with inadequate charging infrastructure makes them attractive for modern transportation networks [5]. Photovoltaic (PV) energy is one of the most widely utilized renewable sources in SMPB systems because of its modularity, decreasing installation cost, and environmental benefits [6]. However, PV generation is highly dependent on solar irradiance and weather conditions, leading to intermittent power production and reduced energy availability during cloudy conditions or nighttime operation [7]. Such intermittency can adversely affect dc-bus voltage regulation and system stability, especially when sudden AFV charging demands occur. Therefore, relying solely on PV generation limits the operational reliability of mobile microgrids. To overcome these limitations, researchers have explored hybrid renewable energy systems that combine multiple energy sources to improve power availability and system resilience [8]. Wind energy has emerged as an attractive complementary renewable resource due to its distinct generation characteristics compared with solar energy. In many regions, wind power can continue generating electricity during periods of low solar irradiance, thereby enhancing overall renewable energy utilization [9]. The integration of compact wind energy conversion systems (WECSs) into mobile microgrids can significantly improve energy diversity, reduce renewable power fluctuations, and increase charging reliability for AFVs [10]. In addition to renewable generation, energy storage technologies play a critical role in maintaining power balance within dc microgrids. Because renewable energy sources exhibit variable output characteristics, energy storage systems are required to compensate for generation-demand mismatches and provide voltage stabilization [11]. Traditional battery energy storage systems (BESSs) offer high energy density and long-duration power support but exhibit limited capability in handling rapid transient power fluctuations [12]. Conversely, supercapacitors provide excellent power density and fast response characteristics but possess limited energy storage capacity [13]. To exploit the advantages of both technologies, Hybrid Energy Storage Systems (HESSs), consisting of batteries and supercapacitors, have been widely adopted in renewable-energy-based microgrids and EV charging applications [14]. HESS configurations effectively improve power-sharing performance, enhance battery lifetime, and mitigate transient disturbances caused by sudden load changes [15]. The increasing penetration of converter-interfaced renewable energy sources has also introduced new challenges related to system inertia and stability. Unlike conventional synchronous generators, power electronic converters contribute little inherent inertia to the grid, making dc microgrids highly susceptible to voltage oscillations and transient disturbances [16]. To address this issue, Virtual Inertia Control (VIC) techniques have been proposed to emulate the inertial behavior of conventional rotating machines through converter control strategies [17]. VIC improves dynamic performance and provides temporary support during sudden power imbalances. However, fixed-parameter VIC approaches may not adequately respond to rapidly changing operating conditions, particularly in mobile microgrids characterized by highly variable AFV charging patterns and renewable power fluctuations [18]. Recent advances in artificial intelligence and machine learning have opened new opportunities for enhancing microgrid control and energy management. Artificial Neural Networks (ANNs) have demonstrated excellent capability in

nonlinear system identification, adaptive control, and real-time decision-making [19]. Unlike conventional control techniques that rely on predefined mathematical models, ANN-based controllers can learn system behavior from operating data and continuously adapt control actions to changing environmental and load conditions. This adaptive capability makes ANN controllers particularly suitable for renewable-energy-based microgrids, where uncertainty and variability are inherent characteristics [20]. Several studies have investigated ANN applications for dc-bus voltage regulation, power-sharing optimization, and energy management in microgrids. These intelligent controllers have shown improved transient response, reduced voltage deviations, and enhanced robustness against parameter variations compared with conventional proportional-integral (PI) and virtual inertia-based controllers [21]. Furthermore, ANN-based energy management strategies can effectively coordinate multiple distributed energy resources and storage units, resulting in improved renewable energy utilization and reduced dependency on utility grid support [22]. Despite significant progress in renewable-energy-powered charging infrastructures, existing SMPB architectures generally rely on PV generation combined with HESS and conventional control approaches. Such systems remain vulnerable to prolonged low-solar conditions and may experience degraded performance during sudden AFV charging or discharging events [23]. Moreover, the integration of wind energy and adaptive intelligent control within a unified SMPB framework has received relatively limited attention in the literature. To address these challenges, this paper proposes an enhanced Smart Mobile Power Bank architecture incorporating a hybrid Wind–PV–HESS system coordinated through an adaptive Artificial Neural Network controller. The proposed design integrates a compact Wind Energy Conversion System (WECS) alongside the conventional PV generation unit to provide complementary renewable power support. A battery–supercapacitor HESS is employed to improve energy balancing and transient power compensation. The adaptive ANN controller continuously learns operating conditions and dynamically coordinates power flow among the wind generator, PV array, HESS, and grid-interfaced converters. The primary objectives of the proposed system are to improve dc-bus voltage regulation, reduce transient oscillations, enhance renewable energy utilization, and minimize utility-grid dependency under varying AFV charging demands. In addition, the SMPB is designed to function not only as a mobile charging station but also as a grid-supportive dc machine capable of providing voltage smoothing, inertia emulation, and ancillary support services. Simulation studies demonstrate that the proposed Wind–PV–HESS-based SMPB with adaptive ANN control achieves superior dynamic performance and operational stability compared with conventional VIC-based approaches.

2. System Configuration

The proposed Enhanced Smart Mobile Power Bank (SMPB) is designed as a mobile DC microgrid integrating a Photovoltaic (PV) system, Wind Energy Conversion System (WECS), Hybrid Energy Storage System (HESS), grid-interface converter, and Alternative Fuel Vehicle (AFV) charging station. The PV array and wind turbine serve as complementary renewable energy sources, providing continuous power generation under varying environmental conditions. A Hybrid Energy Storage System consisting of a battery and supercapacitor is employed to store excess renewable energy, compensate power fluctuations, and maintain DC-bus voltage stability. All components are interconnected through a common DC bus, which acts as the central power exchange platform. A bidirectional Voltage Source Converter (VSC) enables power transfer between the SMPB and the utility grid, allowing both grid-support and charging operations. An adaptive Artificial Neural Network (ANN) controller continuously monitors system conditions and coordinates power flow among the PV system, WECS, HESS, grid, and AFV loads. This integrated configuration improves renewable energy utilization, enhances dynamic performance, reduces transient disturbances, and minimizes dependence on the utility grid during AFV charging and discharging operations.

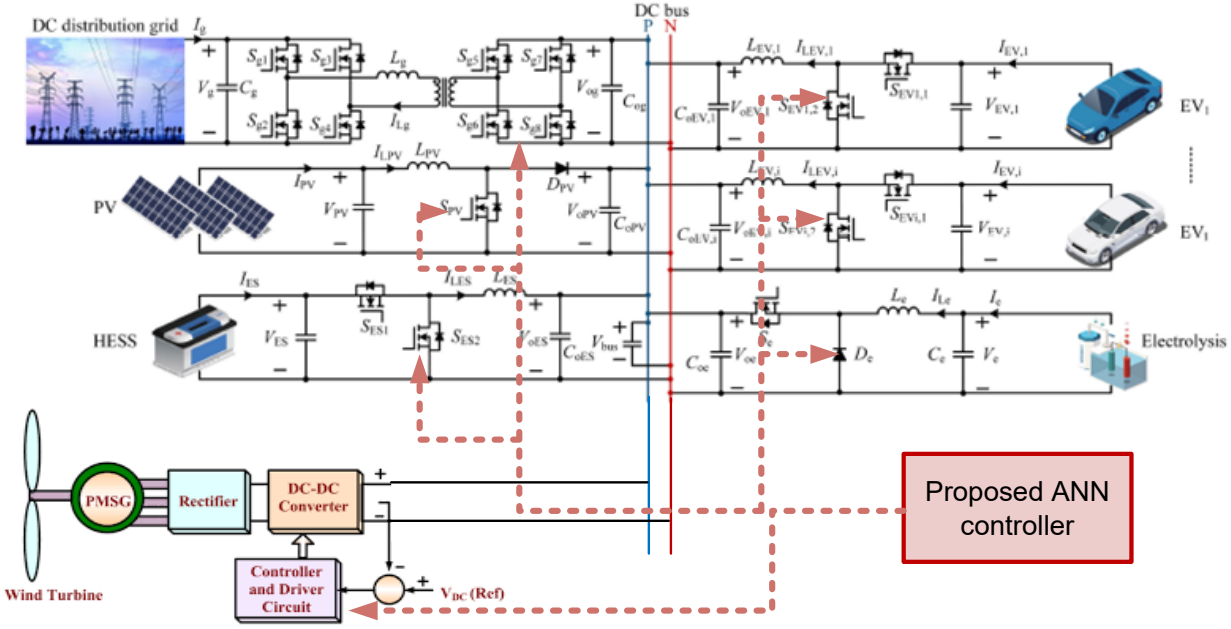

Fig. 1 System structure of the Proposed SMPB

3. Operating Modes of the Proposed SMPB

The proposed Smart Mobile Power Bank (SMPB) operates under four different modes depending on the availability of renewable energy sources, the state of charge of the Hybrid Energy Storage System (HESS), AFV charging requirements, and grid conditions. The adaptive ANN controller continuously monitors system parameters and manages power flow to ensure reliable and efficient operation.

1) Mode 1: Grid-Connected Charging Mode

This mode is activated when the SMPB is connected to the utility grid and AFV charging demand is present. The photovoltaic (PV) system, Wind Energy Conversion System (WECS), HESS, and utility grid collectively supply power to the charging loads. The ANN-based energy management system optimally coordinates power sharing among all available sources. During periods of excess renewable generation, surplus energy is stored in the HESS, while additional power can be imported from the grid whenever renewable generation is insufficient to satisfy the charging demand.

2) Mode 2: Mobile Islanded Charging Mode

In this operating mode, the SMPB functions independently from the utility grid and serves as a mobile charging station for AFVs. The PV system, WECS, and HESS supply the required charging power, while the ANN controller maintains DC-bus voltage stability and ensures balanced power distribution. The supercapacitor compensates for rapid power fluctuations, whereas the battery provides sustained energy support, thereby guaranteeing high-quality and uninterrupted charging services.

3) Mode 3: Grid Support Mode

This mode is activated when the utility grid requires additional power support. In this condition, the PV system, WECS, HESS, and connected AFVs participate in supplying power to the grid through the bidirectional converter. The SMPB operates as a grid-supportive DC machine capable of enhancing system stability by providing virtual inertia, voltage regulation, and ancillary services. The ANN controller dynamically regulates power exchange to minimize grid voltage fluctuations and improve overall network reliability.

4) Mode 4: Renewable Energy Storage Mode

This mode occurs when renewable power generation is high and AFV charging demand is low. The available PV and wind power are primarily utilized to charge the HESS and maintain its desired state of charge. If no charging demand exists, excess renewable energy is stored in the battery and supercapacitor units. Once the HESS reaches its maximum storage capacity, surplus renewable energy may be exported to the grid or diverted to auxiliary loads, thereby maximizing renewable energy utilization and minimizing energy wastage. The proposed multi-mode operational strategy enables the SMPB to operate flexibly under varying

environmental and load conditions, ensuring efficient renewable energy utilization, enhanced DC-bus voltage stability, improved power quality, and reduced dependence on the utility grid.

4. MODELING OF SMPB

A. Modeling of HESS

In this work, HESS consists of batteries and SCs. The discharge equation and the charge equation of the lithium battery can be represented as follows:

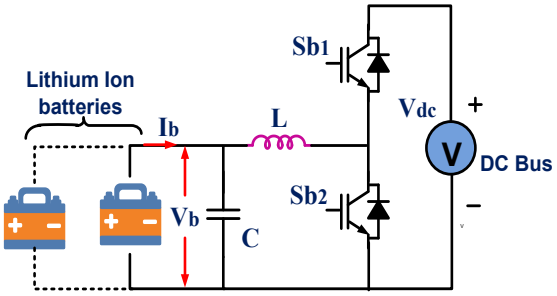

Fig.2 principle operation bidirectional dc-dc buck boost converter

$$f_1(it, i^*, i) = E_0 - \frac{KQ}{Q-it} i^* - \frac{KQ}{Q-it} it + Ae^{-Bit} \quad (1)$$

$$f_2(it, i^*, i) = E_0 - \frac{KQ}{0.1Q-it} i^* - \frac{KQ}{Q-it} it + Ae^{-Bit} \quad (2)$$

where E0 is the initial voltage, K is the polarization resistance, Q is the maximum battery capacity, i∗ is the low-frequency dynamic current, i is the battery current, it is the battery extraction capacity, A is the exponential voltage, and B is the exponential capacity. SoC is used to indicate the remaining capacity of the battery, and the value is defined as the percentage ratio of the remaining capacity to the battery capacity, which is represented as follows:

$$SoC = 100\% \left(1 - \frac{\int_0^1 idt}{Q}\right) (3)$$

The SC can be modeled as follows:

$$V_{sc} = \frac{2N_e N_s RT}{F} \sinh^{-1}\left(\frac{Q_T}{N_P N_e^2 A_i \sqrt{8RT\varepsilon\varepsilon_0 C}}\right) + \frac{N_5 Qrd}{N_P N_e \varepsilon\varepsilon_0 A_i} - R_{SC} I_{SC}$$

(4)

where Vsc is the SC voltage, Ns and Np are the numbers of series and parallel SCs, respectively, Ne is the number of layers of electrodes, QT is the electric charge, d is the molecular radius, and ε and ε0 are the permittivity of material and free space, respectively. R is the ideal gas constant. T is the operating temperature. Ai is the interfacial area between electrodes and electrolyte. C is the molar concentration. F is the Faraday constant. Isc is the SC current. Rsc is the total resistance.

B. Modeling of Water Electrolysis

PEM electrolysis is an electrochemical power conversion device including cathode, anode, and membrane. By applying water electrolysis, water is decomposed into oxygen, hydrogen ions (protons), and electrons at anode. The protons are driven through the PEM to the cathodic catalyst side so as to produce hydrogen by the electric field. The behavior of PEM water electrolysis with ns series cells and np parallel stacks is given [29] as follows:

$$V(T,P) = n_s E_{rev}(T,P) + \frac{n_s}{n_P} I R_1(T,P) \quad (5)$$

where Erev is the reversible voltage and Ri is the initial PEM cell resistance that can be calculated as follows:

$$E_{rev}(T,P) = E_{rev0} + \frac{R_{gas}(2730+T)}{2F} \ln\left(\frac{P}{P_0}\right) \quad (6)$$

$$R_1(T,p) = R_{io} + K \ln\left(\frac{P}{P_0}\right) + dR_1(T - T_0) \quad (7)$$

where Erev0 is the reference reverse voltage at reference temperature (T0) and pressure (p0). In this work, Erev0 is 1.476 V. Rgas is the ideal gas constant, which is 0.082 1 • atm • K−1 • mol−1. F is the Faraday constant, which is 96 487 C • mol−1. k is the curve-fitting parameter that is 0.0395 (V/A). Ri0, T0, and p0 are the reference resistance, temperature, and pressure, respectively. The d Rt ($\Omega \cdot C^{-1}$) is a resistance coefficient of temperature. Ri0 is 0.326 Ω, p is 1 atm, and T0 is 20 ◦C. And d Rt is −3.812 m Ω C−1. C. Modeling of PV The mathematical model of PV cell can be represented as follows:

$$I_{PV} = I_{Ph} - I_d - \frac{V_{PV} + I_{PV} R_{se}}{R_{sh}} \quad (8)$$

where Iph is the photon current, Id is the diode current, and Rsh and Rse are the series and shunt resistances, respectively. Vpv and Ipv are the voltage and current of PV cell, respectively.

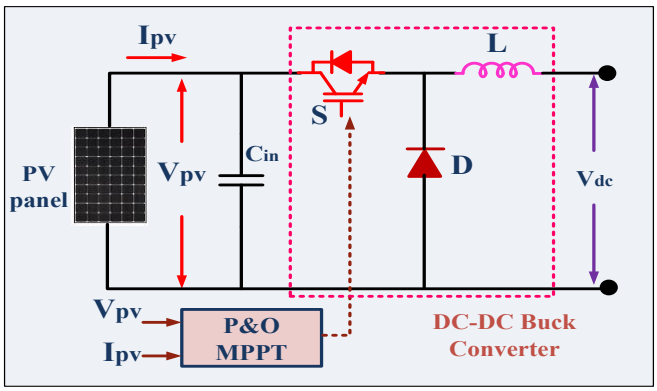

Fig. 3 solar PV P&O MPPT DC-DC Buck converter

1. PV Array Modeling

The output of a solar panel is modeled using the single-diode model, and its output current Ipv is expressed as:

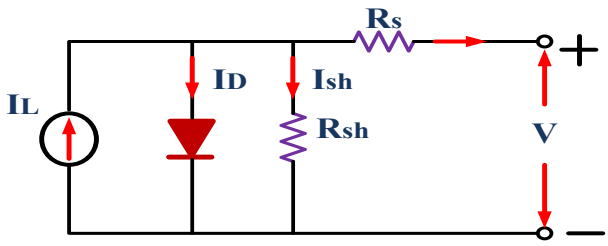

Fig. 4 equivalent model of PV solar.

C. Working and Operation of the PMSG-Based Wind Energy Conversion System

The proposed wind energy conversion system consists of a wind turbine, a Permanent Magnet Synchronous Generator (PMSG), a three-phase diode rectifier, a boost converter, and an MPPT controller. The wind turbine converts wind energy into mechanical energy, which drives the PMSG to generate three-phase AC power. The generated AC voltage is then converted into DC voltage through the three-phase rectifier. The rectified DC voltage (Vw) is filtered by the capacitor Cin and supplied to the boost converter. The boost converter, comprising inductors L1 and L2, switch Sw, diode D, and capacitor Cout, increases and regulates the voltage to maintain the required DC-bus voltage (Vdc). An MPPT controller continuously monitors the wind-side voltage and current and adjusts the duty cycle of the boost converter switch to extract maximum power from the wind turbine under varying wind-speed conditions. Thus, the system efficiently converts variable wind energy into a stable DC output for supplying the DC microgrid, HESS, and AFV charging loads.

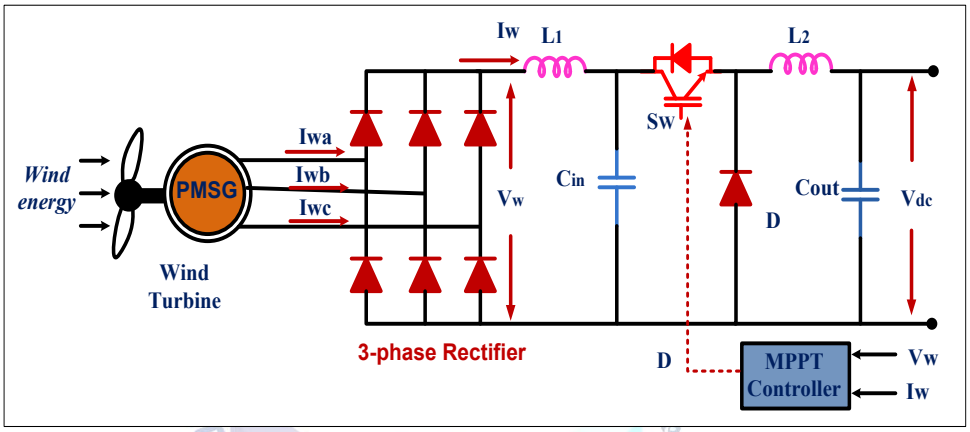

Fig.5 wind conversion topology

5. PROPOSED OPERATION AND CONTROL STRATEGY

Fig. 2 shows the control strategy of SMPB, which consists of power grid controller, EHHRS controller, HESS controller, and PV controller. The different controllers can be used to enable the different operation modes. In all the modes, PV is operated at the maximum power point tracking (MPPT) mode.

A. Operation Mode 1: Grid Supplying Mode

When SMPB is operated in mode 1, the power grid and HESS are used to maintain dc bus voltage. The constant voltage control strategy is adopted for EV and the constant current control strategy is adopted for electrolysis. The power of PV depends on light intensity and is not sufficient. Power grid and HESS provide the remaining required energy to the EHHRS, where the power relationship can be represented as follows:

$$P_g + P_{ES} = P_{EV} + P_h - P_{PV} \qquad (9)$$

where Pg, PES, PEV, Pe, and PPV are the power of grid, HESS, EVs, hydrogen production, and PV, respectively. As shown in Fig. 3, an electricity price-prioritized droop control strategy is developed to perform power management between power grid and HESS in a cost-effective way. The real-time electricity price and SoC are considered to perform operation mode management of HESS as shown in Fig. 4. The constraint of SoC can be given as follows:

$$SoC_{\min} \le SoC_{ES} \le SoC_{\max} \qquad (10)$$

In an HESS with batteries and SCs, equivalent SoC can be defined as the weighted average of SoC values of different energy storage elements to represent the overall charging and discharging characteristics. This work mainly focuses on the external characteristics of HESS, hence, the characteristics of HESS can be represented by equivalent SoC. In this work, the upper and lower limits of SoC are specified as 90% and 20%, respectively. When the SoC of HESS satisfies constraint

(9), improved power-sharing between power grid and HESS can be implemented based on the real-time electricity price, where the droop relationship for power regulation is given as follows:

$$V_{oES.ref} = V^*_{bus} - m_{ES}P_{ES} = V^*_{bus} - \frac{V_{\max}-V_{\min}}{P_{ES,rate}} \quad (11)$$

$$V_{og.ref} = V^*_{bus} - m_g P_g = V^*_{bus} - \frac{\lambda e(V_{\max}-V_{\min})}{P_{g,rate}} P_g$$

$$\lambda_e = \frac{C_t - C_{mean}}{C_{mean}} \quad (12)$$

where VoES,ref and Vog,ref are the reference output voltages of power grid and HESS, respectively, V∗ bus is the rated reference value of dc bus, mES and mg are the droop coefficients of power grid and HESS, respectively, and Vmax and Vmin are the maximum and minimum voltage amplitudes of the dc bus, respectively. ct is the real-time electricity price and cmean is the average electricity price of the previous day. Different from the conventional droop control, the electricity price coefficient λe is introduced into droop coefficient mg to form the proposed droop control equation. The droop coefficient mES is constant. The resulting droop coefficient mg will then be different according to the real-time electricity price. The power-sharing between power grid and HESS thus can be changed as the variation in ct. The power-sharing ratio (η) of power grid and HESS is represented as follows:

$$\eta = \frac{P_g}{P_{ES}} = \frac{P_{g,rate}}{\lambda_e P_{ES,rate}} \quad (13)$$

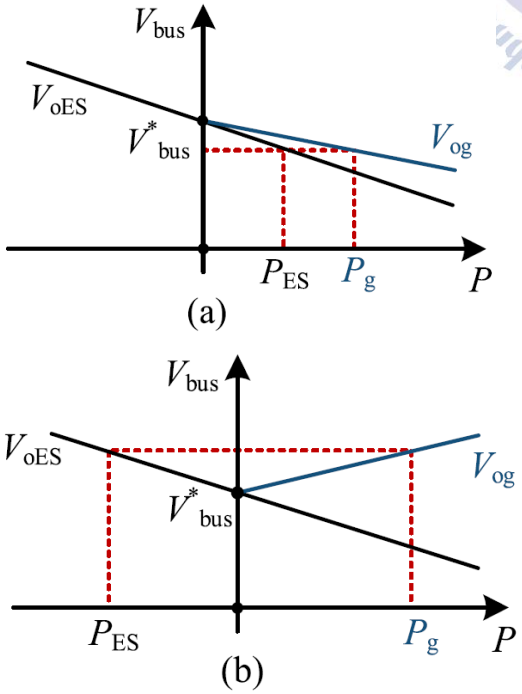

Fig. 6. V–P droop curve of the proposed power controller. (a) HESS: discharge mode. (b) HESS: charge mode.

Fig. 6 shows the droop curve of the proposed power controller. When the electricity price ct is higher than the average electricity price cmean, where λe > 0, HESS is operated in the discharge mode as shown in Fig. 6(a). During this period, the power proportion of power grid is decreased with the increase in electricity price ct . For certain output power, the grid power Pg is decreased with the increase in ct . When ct is lower than cmean, where λe < 0, Fig.6 (b) shows that HESS is operated in the charge mode. During this period, Pg is increased with the decrease in ct . Fig. 6 shows the relationship of Pg, PES, and the electricity price ratio (ct/cmean) when Pg + PES = 500 kW. As shown in Fig. 6, when ct ≤ cmean, power grid supplies HESS. When ct ≥ cmean, power grid and HESS together supply the EHHRS. The power-sharing ratio η is decreased with the increase in ct . The grid power is decreased with the increase in ct.

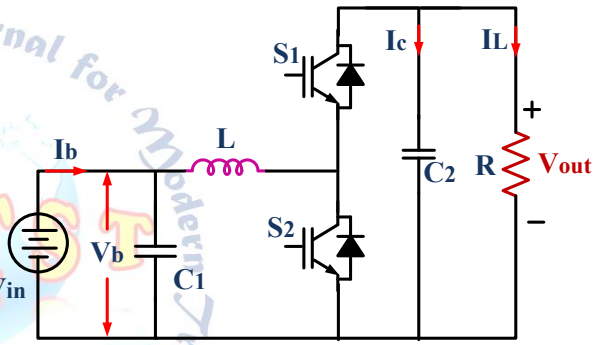

Fig.5 circuit diagram of DC-DC bidirectional buck boost converter

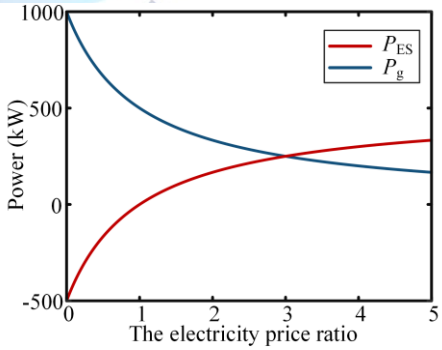

Fig. 6. Relationship of Pg, PES, and ct /cmean.

B. Operation Mode 2: Mobile Islanded Mode In mode 2, the power grid controller is operated in the idle mode, where there is no power exchange with power grid. The constant voltage control strategy is adopted to provide power supply for EVs in this mode. HESS is the main energy source. The HESS controller is used to maintain dc bus voltage by the proposed VIC strategy. To better understand the proposed VIC strategy, the concept of virtual inertia is first introduced and then extended to the proposed strategy. The concept of virtual inertia is

from the rotating mass of synchronous generator represented by the swing (12), which indicate a capability to deal with power imbalance

$$2H\frac{d\omega}{dt} = P_m - P_e - D\Delta_\omega \qquad (14)$$

where D is the damping factor, H is the inertia constant, ω is the per unit frequency, and Pm and Pe are the mechanical power and electrical power, respectively. In the dc system, an analogous representation of the swing equation can be given as follows:

$$P_{o.ref} - P_{Load} = D\Delta V_{bus} + 2H\frac{dV_{bus}}{dt} \qquad (15)$$

where Po,ref and Pload are the output power reference and load power, respectively. During steady-state operation, the output power reference is equivalent to the sum of Pload and the damping power D1Vbus. The dc bus voltage Vdc remains unchanged. In the presence of voltage disturbances, Po,ref is equivalent to the sum of the load power Pload, the damping power D1Vbus, and the virtual inertia power Pvir. Therefore, the rate of change of voltage (RoCoV) of dc bus can be decreased.

A schematic of HESS connected to the dc bus through a bidirectional dc/dc converter is shown in Fig. 5. When the system operates in a steady-state, the dc bus voltage maintains constant, PES = Pload. When the load power fluctuates suddenly, the dc bus capacitor Cdc will discharge or charge due to unbalanced power. Constrained by the actual capacity of Cdc, the SMPB led by power converters has low inertia, so that the dc bus voltage has a large fluctuation. Therefore, the virtual inertia power Pvir is introduced to the HESS to reduce RoCoV of dc bus, which can be obtained as follows:

$$\Delta P_{load} = P_{Vir} + C_{dc}\frac{V_{bus}}{dt} = (C_{Vir} + C_{bus})V_{bus}\frac{dV_{bus}}{dt} \qquad (16)$$

where Cvir is the virtual inertia capacitor. According to (14), the RoCoV of dc bus can be decreased by adding Cvir during a load power fluctuation. The detection of dVbus/dt is always sensitive to noise and harmonic distortion in a practical control system. Furthermore, the switching ripple of converter can cause interference. Therefore, dVbus/dt can be replaced by transient voltage variation δVbus due to small sampling period, and (14) can be modified as follows:

$$P_{Vir} = C_{Vir}V_{bus}(V_{bus} - V_{bus0}) = C_{Vir}V_{bus}\delta V_{bus} \qquad (17)$$

where Vbus0 is the dc bus voltage of the previous sample. Fig. 8 shows the proposed VIC strategy, which is composed of a VIC loop and a conventional voltage/current dual-loop controller. The proposed VIC loop can generate the current reference increment 1I ∗, where 1I ∗ = CvirVbus. The dead zone limit can eliminate the effects of switching ripple. The output of the VIC loop is added to the output of voltage controller to obtain the reference of the internal current controller. The proposed VIC strategy is very easy to integrate into other controllers. In this article, the HESS provides inertia support to dc bus in all the operating modes.

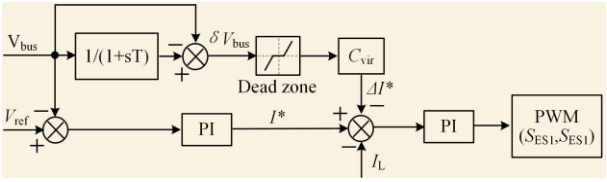

Fig. 7. Proposed VIC strategy for HESS.

C. Operation Mode 3: Grid Supporting Mode

In mode 3, the SMPB is controlled as a voltage source to provide power and inertia support for power grid. The hydrogen electrolysis is operated in the idle mode. EVs can supply the virtual inertia and damping power through the SoC-based VIDC in this mode. HESS can maintain dc bus voltage and provide the remaining required power. The virtual inertia power Pvir can be supplied quickly by swinging the P/V droop curve, and the dynamic swing of the droop curve can be realized. Fig. 9 shows the P/V droop curve with the virtual inertia power. When the converter is operated in steady-state at time t1, the dc bus voltage is V1 and the output power is Po(t1). When PV power is decreased or the load power is increased, the dc grid voltage drops rapidly to V2 at time t2. The operating point of the converter will move from A to B to increase its output power from Po(t1) to Po(t2) under the traditional droop control. During the time instant from t1 to t2, the power difference in the transient process causes the voltage across the output capacitor to drop rapidly, which can cause system instability. To improve the transient response of this system, virtual inertia is added to the droop control. Under the proposed virtual inertia droop control, the power of the converter can immediately increase to Po(t2) + Pvir without a large dc voltage drop at time t2. In addition, when the dc grid voltage rises instantaneously, the output power of the converter is reduced, and Pvid will become negative to suppress the voltage rise. After a voltage fluctuation of dc grid, a new steady-state operating point of the converter will be established. The RoCoV of the dc voltage is significantly reduced.

The SoC-based VIDC strategy is shown in Fig. 8. Grid voltage fluctuations are detected and applied to EV and

grid controllers. The EVs provide virtual inertia and damping power to the dc bus and deliver it to dc grid by the grid converter. According to the above analysis, the improved droop equation can be given as (16), which is applied to the grid controller

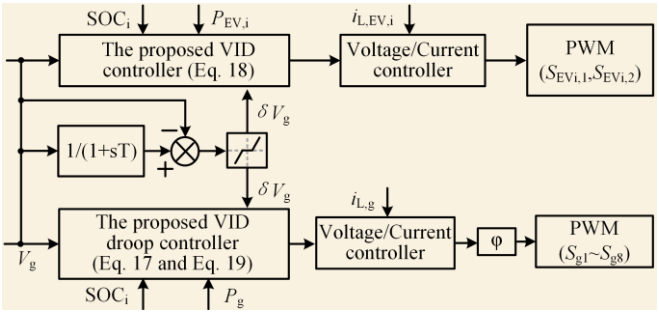

Fig. 8. Proposed SoC-based VIDC strategy.

$$V_g = V_{ref} - D_g\left(P_g - H_g\frac{dV_g}{dt}\right) \qquad (18)$$

where Hg is the inertia constant of grid. Dg is the damping factor of grid. dVbus/dt can represent the transient voltage variation δVbus, and therefore, (16) can be modified as follows:

$$V_g = V_{ref} - D_g(P_g - H_g\delta V_g) \qquad (19)$$

EVs are controlled by constant power output. The SoC of EV is introduced into EV power PEV to form the proposed SoC-based VIDC equation of EV, which is given as follows:

$$P_{EV.i} = (\lambda_{SoC,i})\left(\frac{\Delta V_g}{D_{EV}} + H_{EV}\delta V_g\right)$$

$$\lambda_{SoC,i} = 10SoC_i - 8 \qquad (20)$$

where HEV is the inertia constant of EV. DEV is the damping factor of EV, λSoC,i is the SoC factor of EVi, and SoCi is the SoC of EVi. H is the inertia constant that is a critical factor for RoCoV of the dc bus voltage. The virtual inertia power Pvir is proportional to H at fixed δVg. The virtual inertia power of grid is supplied by EVs. Therefore, the inertia constant of grid (Hg) is the sum of inertia constants of EVi (HEV,i), which can be given as follows:

$$H_g = \sum_{i=1}^{n} SoC_1, H_{Ev}$$

The SoC of the energy storage system is introduced into EV inertia support to perform SoC balancing control by the proposed droop control. The SoC of all the EVs is limited between 80% and 90% in the grid supporting mode. According to (18), λSoC,i can be limited between 0 and 1. When the SoC of the EV is lower than 80%, the EV will no longer provide power support. SMPB will support power grid without affecting the use of EV.

D. Operation Mode 4: Fixed Islanded Mode In mode 4, PV can be enabled to provide power supply of EHHRS and HESS. When the local EV charging demand is low and PV is sufficient, the SMPB can efficiently use the PV to produce green hydrogen in this mode. The HESS can maintain dc bus voltage. The constant current control strategy is adopted for hydrogen electrolysis.

6. Proposed ANN Controller for VdcVoltage Regulation

To enhance the dynamic performance and adaptability of DC-link voltage regulation, an Artificial Neural Network (ANN)-based controller is employed. Unlike conventional controllers, the ANN can effectively handle nonlinearities, uncertainties, and varying operating conditions in hybrid PV–wind–BESS systems.

A. ANN Controller Structure

The ANN used in this work is a feedforward multilayer perceptron (MLP) consisting of an input layer, one hidden layer, and an output layer. The input variables to the ANN are selected as the DC-link voltage error and its rate of change:

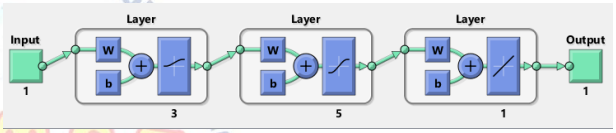

Fig 9: Structure of Neural Network

$$e(k) = V_{dc}^{*} - V_{dc}(k)$$

$$\Delta e(k) = e(k) - e(k-1) \qquad (23), (24)$$

where Vdc∗ is the reference DC-link voltage and Vdc(k) is the measured voltage at instant k.

The ANN output u(k) represents the control signal used to regulate the DC-link voltage through power converters.

$$h_j = f\left(\sum_{j=1}^{n} w_{ij}^{(1)}x_i + b_j^{(2)}\right) \qquad (25)$$

Where

xi = input variables (e,Δe),

wij(1) = weights between input and hidden layer,

bj(1) = bias of hidden neuron,

f(·) = activation function (typically sigmoid or ReLU).

The final ANN output is given by:

$$u(k) = \sum_{j=1}^{m} w_j^{(2)}h_j + b^{(2)} \qquad (26)$$

where

wj(2) = weights from hidden to output layer,

b(2) = output bias.

B. Training of ANN Controller

The ANN is trained using supervised learning to minimize the voltage regulation error. The cost function is defined as:

$$J = \frac{1}{2}e^2(k) \qquad (27)$$

The weights are updated using gradient descent (backpropagation):

$$w^{new} = w^{oid} - \eta \frac{\partial J}{\partial w} \qquad (28)$$

where η is the learning rate.

Training data is generated from system simulations under different operating conditions, including variations in:

- PV irradiance
- Wind speed
- EV load demand
- BESS operating states

C. ANN-Based Control Strategy

The trained ANN generates the control signal u(k), which is used to regulate the DC-link voltage by adjusting the duty cycle of the DC–DC converter or modulation index of the converter. The control objective is to maintain:

$$V_{dc} \approx V_{dc}^{*} \qquad (29)$$

under all operating conditions.

7. Simulation Results and Discussion

The performance of the proposed Wind–PV–HESS integrated Smart Mobile Power Bank (SMPB) with adaptive ANN control was evaluated in MATLAB/Simulink under varying operating conditions. The objective of the simulation study was to analyze the dynamic behavior of the system in terms of grid voltage, grid current, PV output characteristics, DC-bus voltage regulation, and energy storage response during changes in renewable generation and load demand.

A. Grid Voltage and Grid Current Performance

The grid voltage waveform remains balanced and sinusoidal throughout the simulation period, as shown in Fig. 10 (a). The voltage magnitude is maintained at its rated value without noticeable distortion, indicating proper synchronization between the converter and the utility grid. This demonstrates the effectiveness of the ANN controller in maintaining stable operation under varying power conditions. The corresponding grid current waveform is shown in Fig. 10 (b). It can be observed that the current magnitude changes at different instants according to the power demand and renewable power availability. Initially, the grid current is relatively low; however, it increases around 0.3 s and again near 0.6 s due to variations in load demand and power-sharing requirements. Despite these transitions, the current remains sinusoidal and stable, confirming satisfactory power exchange between the SMPB and the utility grid.

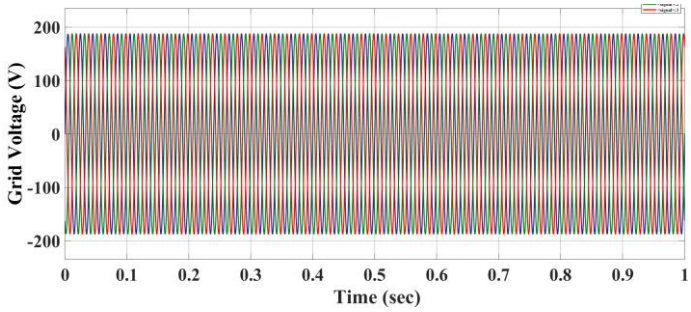

Fig.10 (a) Three-Phase Grid Voltage (Vgrid)

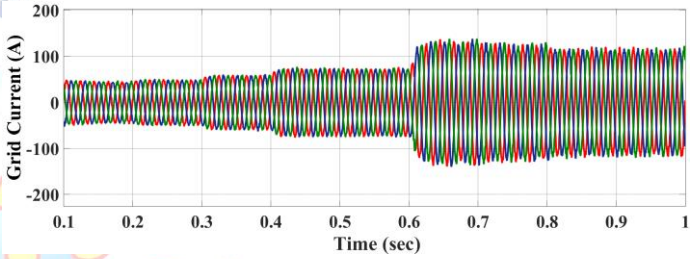

Fig.10 (b) Three-Phase Grid Current (Igrid)

B. PV Voltage and current Characteristics

Fig. X(c) illustrates the PV output voltage (VPV). During the initial startup period, a transient overshoot is observed as the MPPT controller establishes the operating point. After a short settling time, the PV voltage stabilizes at approximately 300 V and remains nearly constant throughout the simulation. The stable voltage profile indicates effective maximum power point tracking and proper operation of the DC–DC converter under varying operating conditions. The PV current waveform is presented in Fig. X(d). The current varies according to changes in solar power generation and load requirements. Initially, the PV current reaches approximately 33 A and subsequently decreases in a stepwise manner due to changes in operating conditions. Around 0.7 s and 0.8 s, the current increases again, indicating increased power extraction from the PV array. The smooth transitions demonstrate the ability of the MPPT controller to track the maximum power point efficiently while maintaining stable operation.

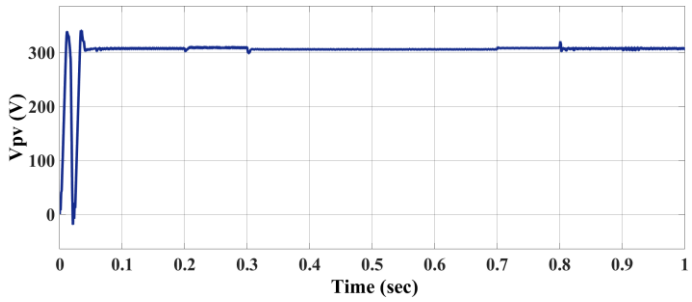

Fig.10 (c) Photovoltaic Output Voltage (VPV)

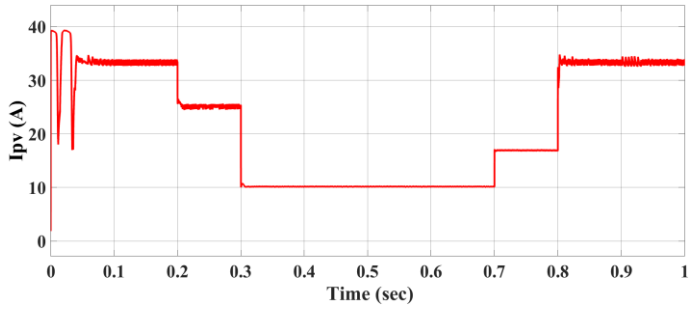

Fig.10 (d) Photovoltaic Output Current (IPV)

D. DC-Bus Voltage Regulation

The DC-bus voltage response is shown in Fig. X(e). At startup, a transient overshoot occurs due to converter initialization and charging of the DC-link capacitor. The voltage quickly settles to approximately 400 V and remains regulated throughout the simulation period. Minor fluctuations are observed during load and power transitions; however, these deviations are effectively suppressed by the ANN controller and HESS coordination. The results confirm the capability of the proposed control strategy to maintain a stable DC bus under dynamic operating conditions.

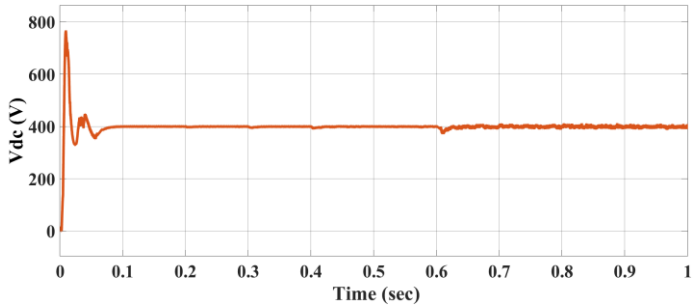

Fig.10 (e) DC-Bus Voltage (Vdc)

E. Electrolysis Current Response

Fig. X(f) shows the electrolyzer current (Iels) of the hydrogen production system. During the initial startup period, the current exhibits a transient response due to system initialization and DC-bus stabilization. After a short settling interval, the electrolysis current rises and stabilizes at approximately 30 A. This indicates that sufficient renewable power is available for hydrogen generation after satisfying the load and storage requirements. The stable current profile demonstrates the effective operation of the electrolyzer and the proposed energy management strategy. As excess power becomes available from the renewable sources, the ANN controller directs the surplus energy to the electrolyzer, enabling efficient hydrogen production while maintaining DC-bus voltage stability. The smooth response of IelsI_{els}Iels confirms that the electrolyzer operates under controlled conditions without causing significant disturbances to the microgrid.

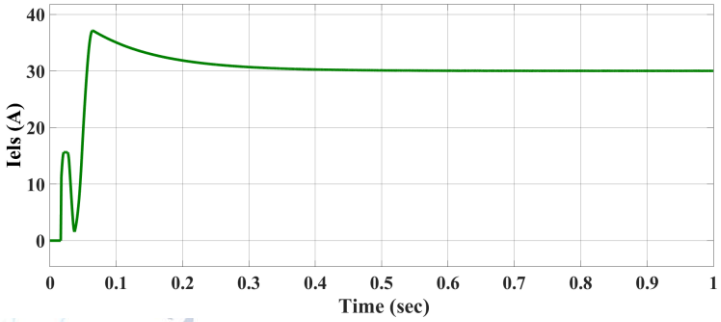

Fig.10 (f) Electrolyzer Current (Iels)

F. Power Sharing Characteristics of the Proposed SMPB

Fig. X(g) illustrates the power-sharing behavior among the utility grid, photovoltaic (PV) system, electrolyzer, and energy storage system (ESS) under varying operating conditions. The black curve represents the grid power, the red curve indicates the PV power, the purple curve corresponds to the electrolysis power, and the green curve shows the ESS power. Initially, the PV system supplies a significant portion of the load demand, reducing the power required from the utility grid. As the operating conditions change, the PV power decreases around 0.4 s and further drops near 0.6 s, indicating variations in renewable energy generation. Consequently, the grid power increases to compensate for the reduction in PV output and maintain power balance within the system. The electrolyzer power remains relatively stable throughout the simulation, demonstrating continuous hydrogen production. Small variations in electrolyzer power are observed during transient conditions, indicating effective energy management and coordinated operation with the renewable sources. The ESS power exhibits dynamic behavior, charging and discharging whenever power imbalance occurs between generation and demand.

Around 0.6 s, the ESS provides additional support to maintain system stability during sudden power transitions. Overall, the results demonstrate that the proposed ANN-controlled Wind–PV–HESS integrated SMPB effectively coordinates power flow among the grid, renewable sources, ESS, and electrolyzer. The intelligent power management strategy ensures stable operation, efficient renewable energy utilization, reliable hydrogen production, and reduced dependence on the utility grid.

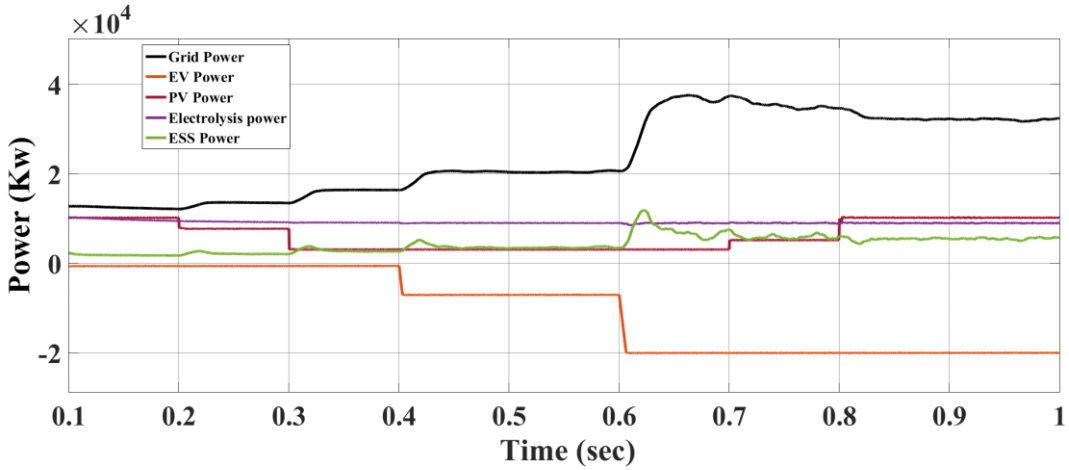

Fig. 10 (g). Power-sharing performance of the proposed SMPB showing grid power, PV power, electrolyzer power, and ESS power.

8. Conclusion

This paper presented an enhanced Smart Mobile Power Bank (SMPB) integrating a Wind Energy Conversion System (WECS), Photovoltaic (PV) generation, and a Hybrid Energy Storage System (HESS) for mobile DC microgrid applications with high penetration of Alternative Fuel Vehicles (AFVs). An adaptive Artificial Neural Network (ANN)-based controller was developed to coordinate power flow among the renewable sources, HESS, electrolyzer, and utility grid while maintaining stable DC-bus operation under varying load and generation conditions. Simulation results demonstrated that the proposed Wind–PV–HESS architecture effectively improves renewable energy utilization, enhances DC-bus voltage regulation, and reduces transient oscillations compared to conventional control approaches. The ANN controller provided fast dynamic response and efficient power management during changes in renewable generation and charging demand. Furthermore, the integration of wind energy increased system reliability during low solar conditions, while the electrolyzer enabled productive utilization of excess renewable power through hydrogen generation. Overall, the proposed SMPB offers a flexible, reliable, and grid-supportive solution for future AFV charging infrastructures and mobile microgrids. The results confirm its capability to reduce grid dependency, improve power quality, and enhance the operational stability of renewable-energy-based charging systems.

Conflict of interest statement

Authors declare that they do not have any conflict of interest.

REFERENCES

[1] H. Yu, Y. Wang, and Z. Chen, "A novel renewable microgrid-enabled metro traction power system—Concepts, framework, and operation strategy," IEEE Trans. Transport. Electrific., vol. 7, no. 3, pp. 1733–1749, Sep. 2021.

[2] Q. Yan, B. Zhang, and M. Kezunovic, "Optimized operational cost reduction for an EV charging station integrated with battery energy storage and PV generation," IEEE Trans. Smart Grid, vol. 10, no. 2, pp. 2096–2106, Mar. 2019.

[3] V. Chamola, A. Sancheti, S. Chakravarty, N. Kumar, and M. Guizani, "An IoT and edge computing based framework for charge scheduling and EV selection in V2G systems," IEEE Trans. Veh. Technol., vol. 69, no. 10, pp. 10569–10580, Oct. 2020.

[4] J. Singh and R. Tiwari, "Cost benefit analysis for V2G implementation of electric vehicles in distribution system," IEEE Trans. Ind. Appl., vol. 56, no. 5, pp. 5963–5973, Sep. 2020.

[5] R. P. Upputuri and B. Subudhi, "A comprehensive review and performance evaluation of bidirectional charger topologies for V2G/G2 V operations in EV applications," IEEE Trans. Transport. Electrific., vol. 10, no. 1, pp. 583–595, Mar. 2024.

[6] P. Li, W. Hu, X. Xu, Q. Huang, Z. Liu, and Z. Chen, "A frequency control strategy of electric vehicles in microgrid using virtual synchronous generator control," Energy, vol. 189, Dec. 2019, Art. no. 116389.

[7] H. Abubakr, T. H. Mohamed, M. M. Hussein, J. M. Guerrero, and G. Agundis-Tinajero, "Adaptive frequency regulation strategy in multiarea microgrids including renewable energy and electric vehicles supported by virtual inertia," Int. J. Electr. Power Energy Syst., vol. 129, Jul. 2021, Art. no. 106814.

[8] K. Dhingra and M. Singh, "Smart charging station to cater the sudden ingress and egress of EVs while supporting the frequency of microgrid through VSG," Arabian J. Sci. Eng., vol. 45, no. 8, pp. 6715–6727, 2020.

[9] S. Ke et al., "A frequency control strategy for EV stations based on MPC-VSG in islanded microgrids," IEEE Trans. Ind. Informat., vol. 20, no. 2, pp. 1819–1831, Feb. 2024, doi: 10.1109/TII.2023.3281658.

[10] Y. Wang, T. John, and B. Xiong, "A two-level coordinated voltage control scheme of electric vehicle chargers in low-voltage distribution networks," Electr. Power Syst. Res., vol. 168, pp. 218–227, Mar. 2019.

[11] X. Xu et al., "Optimal operational strategy for an offgrid hybrid hydrogen/electricity refueling station powered by solar photovoltaics," J. Power Sources, vol. 451, Mar. 2020, Art. no. 227810.

[12] H. Yu, Y. Wang, H. Zhang, and Z. Chen, "Impedance modeling and stability analysis of triple-active-bridge-converter-based renewableelectricity- hydrogen-integrated metro DC traction power system," IEEE Trans. Ind. Electron., vol. 70, no. 12, pp. 12340–12353, Dec. 2023.

[13] J. Lin et al., "A power factors full-dimensionally hunted power distribution strategy for railway power flow controller considering regenerative braking," IEEE Trans. Ind. Informat., vol. 20, no. 1, pp. 138–148, Jan. 2024.

[14] J. Lin, S. Hu, Y. Li, J. Zhang, J. Zhang, and J. Yu, "A frameworkcompatible hierarchical railway power regulation strategy with the integration of energy storage-embedded railway power flow controller," IEEE Trans. Transport. Electrific., early access, Nov. 27, 2023, doi: 10.1109/TTE.2023.3337268.

[15] P. Garcia-Trivi no, J. P. Torreglosa, L. M. Fernandez-Ramirez, and F. Jurado, "Control and operation of power sources in a medium-voltage direct-current microgrid for an electric vehicle fast charging station with a photovoltaic and a battery energy storage system," Energy, vol. 115, pp. 38–48, Nov. 2016.

[16] C. Wang, Y. Liu, X. Li, L. Guo, L. Qiao, and H. Lu, "Energy management system for stand-alone diesel-wind-biomass microgrid with energy storage system," Energy, vol. 97, pp. 90–104, Feb. 2016.

[17] A. Zahedmanesh, K. M. Muttaqi, and D. Sutanto, "A cooperative energy management in a virtual energy hub of an electric transportation system powered by PV generation and energy storage," IEEE Trans. Transport. Electrific., vol. 7, no. 3, pp. 1123–1133, Sep. 2021.

[18] X. Zhu, M. Xia, and H.-D. Chiang, "Coordinated sectional droop charging control for EV aggregator enhancing frequency stability of microgrid with high penetration of renewable energy sources," Appl. Energy, vol. 210, pp. 936–943, Jan. 2018.

[19] R. Wang, H. Wang, K. Zhu, C. Yi, P. Wang, and D. Niyato, "Mobile charging services for the internet of electric vehicles: Concepts, scenarios, and challenges," IEEE Veh. Technol. Mag., vol. 18, no. 3, pp. 110–119, Sep. 2023.

[20] U. Qureshi, A. Ghosh, and B. K. Panigrahi, "Scheduling and routing of mobile charging stations with stochastic travel times to service heterogeneous spatiotemporal electric vehicle charging requests with time windows," IEEE Trans. Ind. Appl., vol. 58, no. 5, pp. 6546–6556, Sep. 2022.

[21] M. O. Badawy et al., "Design and implementation of a 75-kW mobile charging system for electric vehicles," IEEE Trans. Ind. Appl., vol. 52, no. 1, pp. 369–377, Jan. 2016.

[22] J. Chen, C. Yi, R. Wang, K. Zhu, and J. Cai, "Learning aided joint sensor activation and mobile charging vehicle scheduling for energy-efficient WRSN-based industrial IoT," IEEE Trans. Veh. Technol., vol. 72, no. 4, pp. 5064–5078, Apr. 2023.

[23] S. Huang, L. He, Y. Gu, K. Wood, and S. Benjaafar, "Design of a mobile charging service for electric vehicles in an urban environment," IEEE Trans. Intell. Transp. Syst., vol. 16, no. 2, pp. 787–798, Apr. 2015.